ACS APPLIED MATERIALS & INTERFACES

Research Article

www.acsami.org

Hierarchical NiAl Layered Double Hydroxide/Multiwalled Carbon Nanotube/Nickel Foam Electrodes with Excellent Pseudocapacitive Properties

Bo Wang,[†] Gareth R. Williams,[‡] Zheng Chang,[†] Meihong Jiang,[†] Junfeng Liu,[†] Xiaodong Lei,*[,†] and Xiaoming Sun[†]

[†]State Key Laboratory of Chemical Resource Engineering, Beijing University of Chemical Technology, P.O. Box 98, Beijing 100029, China

[‡]UCL School of Pharmacy, University College London, 29-39 Brunswick Square, London WC1N 1AX, U.K.

ABSTRACT: The performances of pseudocapacitors usually depend heavily on their hierarchical architectures and composition. Herein, we report a three-dimensional hierarchical NiAl layered double hydroxide/multiwalled carbon nanotube/nickel foam (NiAl–LDH/MWCNT/NF) electrode prepared by a facile three-step fabrication method: in situ hydrothermal growth of NiAl–LDH film on a Ni foam, followed by direct chemical vapor deposition growth of dense MWCNTs onto the NiAl–LDH film, and finally the growth of NiAl–LDH onto the surface of the MWCNTs via an in situ hydrothermal process in the presence of surfactant sodium dodecyl sulfate. The MWCNT surface was fully covered by NiAl–LDH hexagonal platelets, and this hierarchical architecture led to a much enhanced capacitance. The NiAl–LDH/MWCNT/NF electrode has an areal loading mass of 5.8 mg of LDH per cm^2 of MWCNT/NF surface. It also possesses exceptional areal capacitance (7.5 F cm^{-2}), specific capacitance (1293 F g^{-1}), and cycling stability (83% of its initial value was preserved after 1000 charge–discharge cycles). The NiAl–LDH/MWCNT/NF material is thus a highly promising electrode with potential applications in electrochemical energy storage.

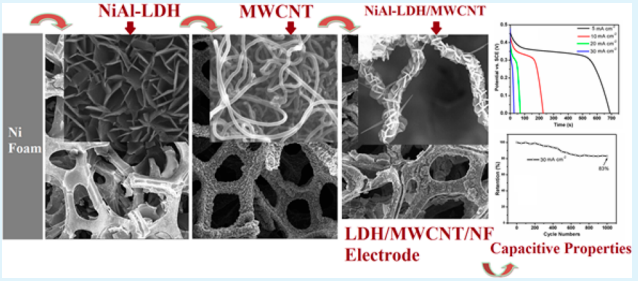

KEYWORDS: *layered double hydroxide, multiwalled carbon nanotube, nickel foam, pseudocapacitor*

1. INTRODUCTON

High–capacitance electrochemical energy storage devices (including supercapacitors and lithium-ion batteries) have been heavily explored and continue to attract very significant research interest, particularly in light of growing requirements for renewable clean energy. Supercapacitors, also called electrochemical capacitors, have high energy density, rapid charge/discharge rates, and long cycle lives compared to conventional dielectric capacitors and traditional secondary batteries.[1−4] Supercapacitors are considered to be very potent potential energy storage devices due to their high power densities and long lifespan.[5−7] At present, commercial supercapacitors are most commonly symmetric electric double-layer capacitors (EDLCs) derived from high surface area carbon materials.[4] However, carbon-based materials suffer from the limitation of low energy density. This is because they store charges electrostatically at their surfaces, which leads to inherently low specific areal capacitance (C_a; around 20 μF cm^{-2}).[8] Transition-metal oxides and hydroxides store charges differently, through surface Faradaic redox reactions. This feature endows them with higher energy density than carbon materials. For example, NiO,[9] Co_3O_4,[10−12] MnO_2,[13] RuO_2,[14] $Co(OH)_2$,[15] and $Ni(OH)_2$[16−18] have recently been considered as candidates for pseudocapacitor electrode materials. However, the relatively low specific capacitance of NiO, Co_3O_4, and MnO_2 and the high cost of RuO_2 greatly limit their applications.[19−22] As a result, mixed-metal oxides/hydroxides attracted much attention in the design of high energy density charge storage materials. Significant work has been devoted to the rational synthesis of advanced heterostructures, with fascinating synergetic properties offered by composite nanostructures. For example, Co_3O_4@$Ni(OH)_2$,[23] Co_3O_4@MnO_2,[24] Co_3O_4/NiO, and ZnO/NiO[25] exhibit excellent specific capacitance and good cycling stability and show great potential for electrochemical energy storage applications.

Layered double hydroxides (LDHs), also known as hydrotalcite-like materials, are two-dimensional materials comprising mixed metal hydroxide layers with charge-balancing anions located in the interlayer space. They are generally expressed by the generic formula $[M^{2+}_{1-x}M^{3+}_{x}(OH)_2]A^{n-}_{x/n}{\cdot}yH_2O$ (M^{2+} and M^{3+} represent divalent and trivalent cations, respectively; A^{n-} is the interlayer anion).[26−28] Recently, much attention has been paid to the use of LDHs containing transition-metal elements as supercapacitor electrode materials. This interest arises as a

Received: July 11, 2014
Accepted: September 3, 2014
Published: September 3, 2014

   dx.doi.org/10.1021/am504530e | ACS Appl. Mater. Interfaces 2014, 6, 16304−16311

result of their possessing relatively high redox activity and being environmentally friendly and because the layered structure of the LDHs provides for a homogeneous dispersion of transition-metal ions, allowing them to be effectively exploited in electrochemical processes.[29] For example, a continuous CoAl−LDH thin film electrode has been fabricated by drying an almost-transparent colloidal solution of CoAl−LDH nanosheets on an indium tin oxide-coated glass plate substrate. The resultant composite has a large specific capacitance of 833 F g^{-1}.[30] Wang's group has found that electrodes consisting of petal-like NiAl−LDH coated on the surface of nickel foam and NiAl−LDH/graphene composites have specific capacitances of 795 and 781.5 F g^{-1}, respectively.[31,32] However, the preparation methods required to prepare the above materials are two-step processes requiring the formation of LDH aggregates in aqueous solution, followed by their deposition or coating onto substrates. The films thereby obtained adhere poorly to the substrate surface and tend to be low-density with many defects. These issues limit their application in supercapacitors.

Although LDHs have been investigated widely and have great potential use as supercapacitors, their electrochemical behavior is usually not sufficient to meet the demands of new energy storage devices, because their electrical conductivity is very poor. Moreover, before LDH powders are used as electrode materials, they must be glued using a binder such as polytetrafluoroethylene (PTFE) and then pressed onto conductive substrates.[31,32] If active LDH materials are grown on the conductive substrate, the as-obtained materials can be directly used as electrodes. This greatly simplifies the manufacturing process. In our group, NiTi−LDH has been synthesized on the surface of Ni foam, and the resultant composite possesses a high areal capacitance of 10.37 F cm^{-2} at 5 mA cm^{-2}.[33] In another study, β-$Ni(OH)_2$ has been constructed into a 3D mesoporous film on Ni foam; this material shows an ultrahigh specific capacitance of 2675 F g^{-1}.[34] Hierarchical $Ni_{0.25}Co_{0.75}(OH)_2$ nanostructured arrays display a high areal capacitance of 9.59 F cm^{-2} and a high specific capacitance of 928.4 F g^{-1} at 5 mA cm^{-2}.[35] In another example, hierarchical Co_3O_4 nanosheet@nanowire arrays provide an elevated specific capacitance of 715 F g^{-1}.[36] NiAl−LDH and carbon nanoparticle composites also demonstrate a large specific capacitance of up to 1146 F g^{-1}.[37]

The association of low-dimensional nanomaterials with two or more levels can result in 3D hierarchical nanocomposites. The combination of carbon materials and LDH flakes leads to the formation of hierarchical composites that can combine the advantages of double-layer and pseudocapacitance. Further, some transition-metal ions, such as Ni, Co, Mn, etc., can be evenly distributed in the LDH layers on the atomic level. This results in high activity in Faradaic redox reactions.[38] Nanocomposites derived from carbon nanotubes and LDHs have exhibited outstanding performance in energy storage.[39]

On the basis of the above considerations, here, we report a hierarchical electrode built from NiAl−LDH, multiwalled carbon nanotubes (MWCNTs), and Ni foam. The electrode was prepared by a three-step method. First, a NiAl−LDH film was grown on the surface of Ni foam. This was then used to catalyze MWCNT production, and subsequently, a NiAl−LDH film was deposited on these tubes. The structural, morphological, and supercapacitive properties of the composite are investigated. This composite has a high specific capacitance and good cycling stability, and the presence of carbon nanotubes enhanced the capacitance and electroactivity of the composite material synthesized. The obtained results will help to amend and construct NiAl−LDH/MWCNT/NF electrodes according to energy storage applications.

2. EXPERIMENTAL SECTION

Materials. Nickel foams (purity: >99.5%) with a size of ca. 30 mm × 20 mm × 1.0 mm were obtained from the Kunshan Desi Electronic Technology Co., Ltd. They were cleaned ultrasonically in a 37 wt % HCl solution for 5 min and washed with deionized water and absolute ethanol, before being dried in an oven at 60 °C. All other reagents were analytical grade and purchased from the Beijing Chemical Reagent Company.

Preparation of NiAl−LDH Film. A piece of treated Ni foam was used as the substrate for NiAl−LDH film formation. $Ni(NO_3)_2{\cdot}6H_2O$ (0.0045 mol) and $Al(NO_3)_3{\cdot}9H_2O$ (0.0015 mol) were dissolved in deionized water (40 mL) and 0.02 mol of urea. The solution was then transferred to a 50 mL Teflon-lined autoclave and heated at 120 °C for 10 h. The resultant product (NiAl−LDH/NF) was washed with deionized water three times and dried at 60 °C for 12 h in air.

Growth of MWCNT/NF Film. A multiwalled carbon nanotube (MWCNT)/Ni foam (NF) film was synthesized in a quartz tube mounted in a horizontal tube furnace. The furnace is equipped with a mass controller and temperature-programmed controller. The MWCNT/NF film was generated via catalytic chemical vapor deposition (CCVD) of acetylene (C_2H_2). The NiAl−LDH film samples were loaded into a ceramic boat, and the furnace temperature was raised to 500 °C at 5 °C min^{-1} under a nitrogen flow (flow rate: 60 standard-state cm^3 min^{-1} (sccm)). Upon reaching 500 °C, H_2 gas (6 sccm) was introduced to the system, and the temperature was maintained at 500 °C for 40 min. The H_2 gas flow was then switched off, and the furnace was heated to 700 °C, before C_2H_2 gas was supplied at a flow rate of 6 sccm. The sample was held at 700 °C for 60 min. After the reaction, the flow of N_2 gas continued while the furnace was cooled to room temperature. The resultant black film was collected from the ceramic boat (and is denoted WMCNT/NF).

Synthesis of NiAl−LDH/WMCNT/NF Electrode. A 0.0045 mol portion of $Ni(NO_3)_2{\cdot}6H_2O$ and 0.0015 mol of $Al(NO_3)_3{\cdot}9H_2O$ were dissolved in 40 mL of H_2O and 0.02 mol of urea. The solution was magnetically stirred for 10 min in air at room temperature. The surfactant sodium dodecyl sulfate (SDS; 10 mg) was added to the solution, and vigorous stirring continued until the solution was homogeneous. The WMCNT/NF sample and this solution were transferred to a 50 mL Teflon-lined autoclave before being heated at 120 °C for 10 h. After the reaction, the WMCNT/NF film covered with NiAl−LDH was removed from the autoclave, washed with H_2O, and dried at 60 °C for 12 h. This yielded the final electrode (denoted NiAl−LDH/WMCNT/NF).

Characterization. X-ray powder diffraction (XRD) patterns were obtained on a Shimadzu XRD-6000 diffractometer. The instrument is supplied with Cu Kα radiation (λ = 1.5418 Å), and data were collected with a scan speed of 10°/min over the 2θ range from 3° to 70°. The morphologies of samples were analyzed using a field-emission scanning electron microscope (FESEM; Zeiss SUPRA 55) that was operated at 20 kV. Energy-dispersive X-ray spectroscopy (EDX) mapping of the samples was undertaken using an Oxford Link-ISIS 300 EDX attachment. High-resolution transmission electron microscope (HRTEM) observations were carried out on a JEOL JEM-2100 instrument operated at 100 or 200 kV. Fourier transform infrared (FT-IR) spectra were collected with the aid of a Bruker Vector 22 FT-IR spectrometer at a resolution of 4 cm^{-1}. Prior to spectral acquisition, samples were pressed into KBr discs with (weight ratio of sample to KBr: 1:100). Inductively coupled plasma - optical emission spectroscopy (ICP) was undertaken using a Shimadzu ICPS-7500 instrument. Samples were prepared by dissolving the NiAl−LDH in a nitric acid solution (mass fraction: 1%). Raman spectra were obtained at room temperature on a confocal Raman spectrometer (Jobin-Yvon Horiba HR800). This instrument uses an Ar^+ laser of 532 nm wavelength as an excitation source. The laser (output power: 10 mW) was focused on the sample surface. Electrochemical measurements were carried out

at 298 K in a three-electrode glass cell connected to an electrochemical workstation. The electrode (NiAl–LDH/WMCNT/NF, MWCNT/NF, or NiAl–LDH/NF; 1 cm^2) was used as the working electrode. A platinum electrode (1 cm^2) and a saturated calomel electrode were employed, respectively, as counter and reference electrodes. The electrolyte comprised a 1 mol L^{-1} aqueous KOH solution. The workstation was a CHI660D (Chen Hua, Shang Hai) instrument, which can be used for cyclic voltammetry (CV), electrochemical impedance spectroscopy (EIS), galvanostatic charge–discharge, and chronopotentiometry (CP) tests. The Nyquist plots of the electrodes were measured at 0.3 V in the frequency range of $0.01–10^5$ Hz.

3. RESULTS AND DISCUSSION

Structure and Morphology. After hydrothermal treatment in the autoclave, a dense and continuous film of NiAl–LDH crystallites with their [00*l*] direction (or *ab* plane) perpendicular to the surface of the Ni foam substrate is obtained (Figure 1A,B). NiAl–LDH sheets were precipitated

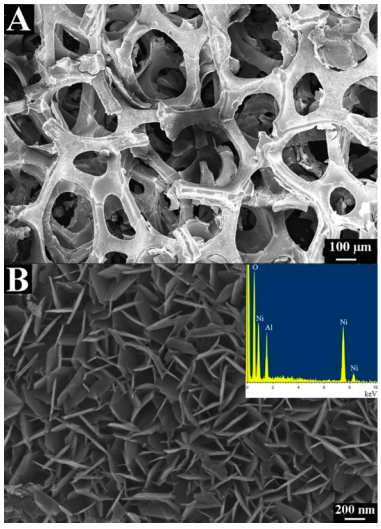

Figure 1. FESEM images (A, B) of the NiAl–LDH film sample. The inset in (B) is the EDX pattern of the film.

from homogeneous solutions by dint of the temperature-controlled hydrolysis of urea. This process leads to a gentle increase in the concentration of carbonate ions and, because of concomitant ammonia formation, solution pH as the reaction proceeds. The result is well-crystallized LDH sheets with large particle sizes in the range of 200–400 nm forming on the substrate. The inset in Figure 1B shows the EDX pattern of the NiAl–LDH film. The Ni/Al molar ratio was determined to be around 2.46. Elemental analysis by ICP showed that the Ni/Al molar ratio in the film was approximately 2.38, in agreement with the EDX measurements.

In XRD, weak, but distinctive, LDH reflections can be seen to be superimposed on the pattern of the Ni foam substrate (Figure 2A). Comparison of the XRD pattern of the film with the powder scraped from the substrate reveals that the peaks can be indexed as the (003), (006), (012), (015), (018), (110), and (113) reflections of a NiAl–LDH phase.[31,32] The FT-IR spectrum of the powder scraped from the NiAl–LDH films (Figure 2B) showed a characteristic intense peak due to the interlayer carbonate ion [$\nu_3(CO_3)$] at 1358 cm^{-1}. The combined results from XRD, IR, SEM, and EDX thus clearly demonstrate that a NiAl–LDH film was formed on the surface of the Ni foam.

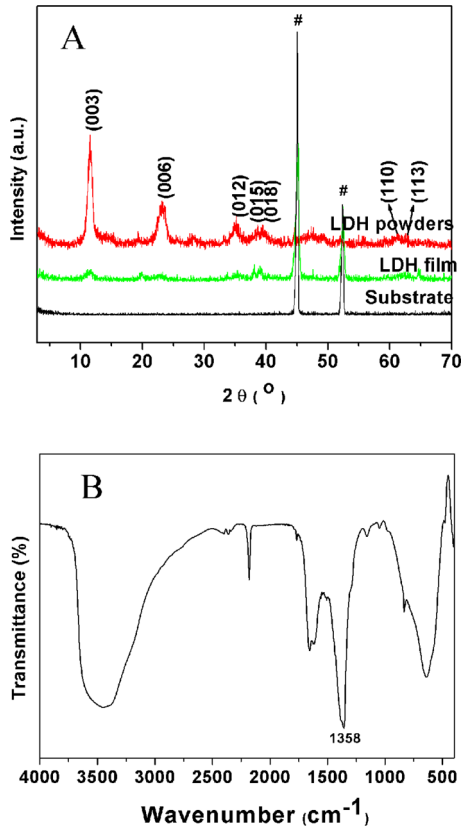

Figure 2. XRD patterns of the Ni foam substrate, NiAl–LDH film, and LDH powder scraped from film samples (A), and the FT-IR spectrum of the powder scraped from the NiAl–LDH films (B).

Panels (C) and (D) in Figure 3 are FESEM micrographs of the MWCNT/NF sample. The MWCNT/NF film has a 3D network structure, the surface of which is rather rough (Figure 3C). If the nickel foam is directly used as the support for in situ growth of carbon nanotubes, the Ni foam substrate would be destroyed because of the very high density of active catalytic Ni atoms and hydrogen embrittlement. In the temperature range of 500–700 °C, the preformed NiAl–LDH film is decomposed and Ni^{2+} ions can be reduced to metallic Ni. It should be noted that the formation of small metallic Ni nanoparticles dispersed in a spinel matrix is possible under these conditions.[40] When these Ni nanoparticles are used as a catalyst for in situ growth of MWCNTs, they can facilitate the growth of an MWCNT film with suitable density. At the same time, the hydrogen embrittlement of Ni foam is prevented and the mechanical performance of Ni foam is changed a little. It is because of oxides and spinel covered on the surface of nickel foam. Black products formed on the surface of Ni foam, as shown in Figure 3A,B. Since the Ni foam is flexible, the MWCNT/NF film can be folded in and out. Panels (A) and (B) in Figure 3 show that the mechanical performance of the Ni foam is not changed. Especially, even repeated folding did not disrupt the black surface of the Ni foam (Figure 3B), indicating the existence of strong interaction between the MWCNTs and the substrate. The FESEM micrographs depict the micrograph of part of one as-grown MWCNT. The nanotube wall is made of more than 10 graphite sheets, typical of multiwalled nanotubes with hollow centers. The graphite sheets are well substrate without any evident damage (Figure 3E). Figure 3D shows that the length of the MWCNTs is several tens of microns. Figure 3E

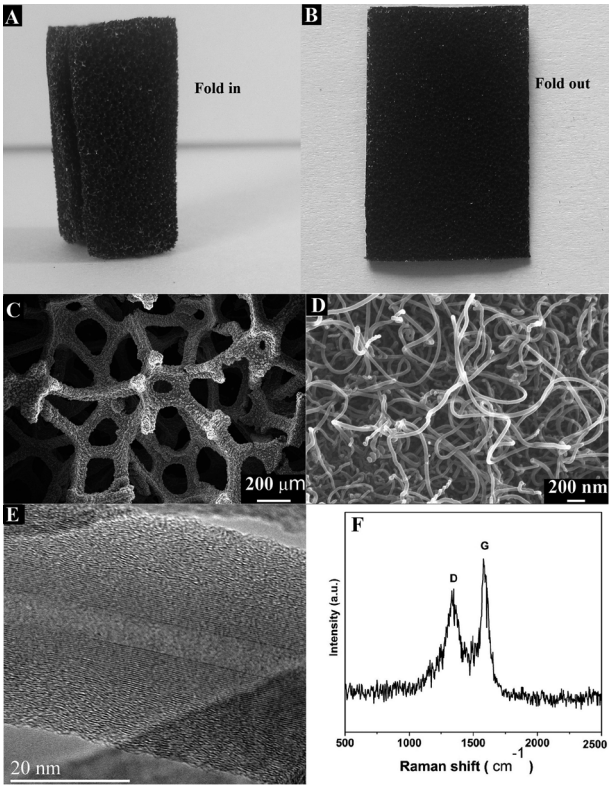

Figure 3. Images of an MWCNT/NF sample after fold in (A) and after fold out (B), FESEM images of MWCNT/NF (C, D), and HRTEM of MWCNT on MWCNT/NF (E), together with a typical Raman spectrum (F).

displays a HRTEM aligned along the axis of the tube. The outer and inner diameters of the MWCNT are ca. 30 and 4 nm, respectively (Figure 3E). Note that the MWCNTs have amorphous carbon on their wall surfaces, but no independent amorphous carbon nanoparticles can be seen in the SEM image (Figure 3D), indicating that the as-grown MWCNTs have high purity.

Further structural studies on the MWCN/NF material have been undertaken with the aid of Raman spectroscopy. Given the lack of homogeneity of MWCNTs, spectra were collected from 10 different parts of the sample to obtain an average of the spectra. Figure 3F shows a representative Raman spectrum of the MWCNT/NF sample. Two major bands are observed, corresponding to the D and G bands of carbon. The G band is found at 1585 cm^{-1} and is related to the vibrations of sp^2-bonded carbon atoms contained in a two-dimensional hexagonal lattice. The observation of this peak thus confirms the formation of the crystalline graphite phase. The D band appears at 1345 cm^{-1} and is demonstrative of carbon atoms with dangling bonds; these arise at the plane terminations of disordered graphite, or in the presence of amorphous carbon.[41,42]

In order to improve the capacitive performance, NiAl−LDH was deposited onto the surface of the MWCNT/NF material. Because MWCNTs are hydrophobic and NiAl−LDH is difficult to grow on hydrophobic surfaces, SDS was added into the reaction solution. NiAl−LDH is formed as hexagonal platelets when urea is slowly hydrolyzed by heating in a Ni^{2+} and Al^{3+} solution.[43,44] When this process was carried out at 120 °C in the presence of MWCNT/NF, the FESEM images (Figure 4) of the resulting material (NiAl−LDH/MWCNT/NF) show

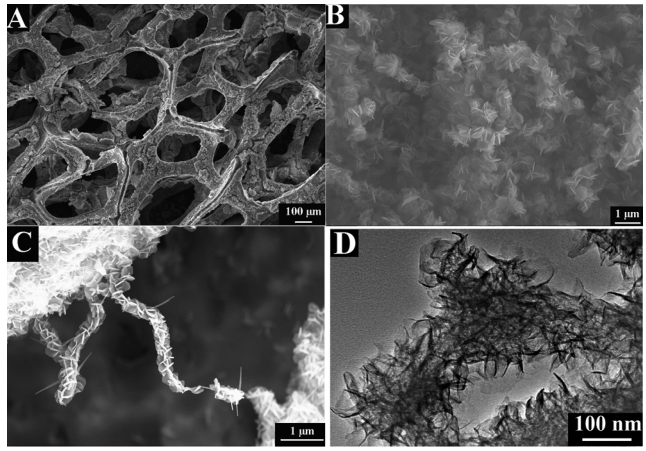

Figure 4. FESEM images of the NiAl−LDH/MWCNT/NF electrode at different magnifications and areas (A−C), and HRTEM image of NiAl−LDH/MWCNT (D).

that a densely packed film of hexagonal LDH platelets covered the tubular MWCNTs. The packing of LDH particles on the surface of the MWCNTs was uniform and close-grained. No uncoated regions of the MWCNTs can be observed. The unique NiAl−LDH/MWCNT core−shell heterostructure is evidenced by HRTEM images (Figure 4D), in which the gauze-like NiAl−LDH sheets are densely grafted throughout the longitudinal axis of the nanotube. Light green NiAl−LDH formed on the surface of MWCNT/NF; even ultrasonication for 2 h did not dislodge it from the MWCNT/NF, also indicating the strong interaction between the NiAl−LDH and the substrate. The load of NiAl−LDH on the film was about 5.8 mg cm^{-2}, calculated by the difference between the weight of NiAl−LDH/MWCNT/NF and MWCNT/NF.

The XRD pattern of the NiAl−LDH/MWCNT/NF electrode is given in Figure 5A. The diffraction peak at about 26.1° can be indexed as the (002) reflection of graphite. The characteristic (003), (006), (012), (015), (018), (110), and (113) reflections of NiAl−LDH[45,46] are also present in the XRD pattern. Two strong diffraction peaks from the Ni foam can be seen at 44.9° and 52.4° (marked "#" in Figure 5A). The Raman spectrum (Figure 5B) of the NiAl−LDH/MWCNT/NF sample conatains peaks at 479, 547, and 1043 cm^{-1} from the NiAl−LDH (cf. Figure 2B) and two signals at 1345 and 1585 cm^{-1} that arise from the MWCNTs. The data presented thus far hence confirm that a 3D hierarchical NiAl−LDH/MWCNT/NF architecture has been generated.

Pseudocapacitive Properties of the NiAl−LDH/MWCNT/NF Electrode. Figure 6A depicts the cyclic voltammogram (CV) of the NiAl−LDH/MWCNT/NF electrode in 1 mol L^{-1} KOH electrolyte at scan rates of 5 and 10 mV s^{-1}. While EDLC electrodes display linear curves, the discharge curves of the NiAl−LDH/MWCNT/NF electrode exhibit typical pseudocapacitive behavior. A pair of redox peaks is observed as a result of the conversion between different oxidation states of Ni:

$$Ni(OH)_2 + OH^- \leftrightarrow NiOOH + H_2O + e^- \quad (1)$$

This involves the intercalation and deintercalation of protons.[47] The discharge curves of the NiAl−LDH/MWCNT/NF electrode at charge/discharge currents densities ranging from 0.0 to 0.48 V are shown in Figure 6B. The specific capacitance was calculated from galvanostatic discharge curves as follows:

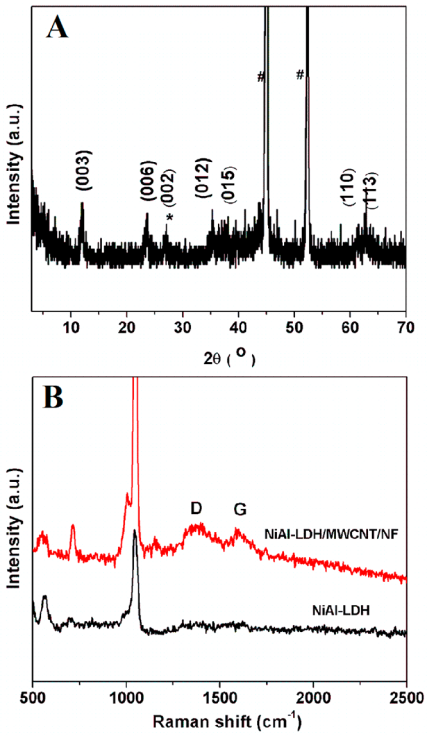

Figure 5. XRD pattern of the NiAl−LDH/MWCNT/NF electrode (A), and Raman spectra of NiAl−LDH/MWCNT/NF and the NiAl−LDH powder (B). The reflection marked ∗ corresponds to graphite, and those denoted with # to the Ni foam.

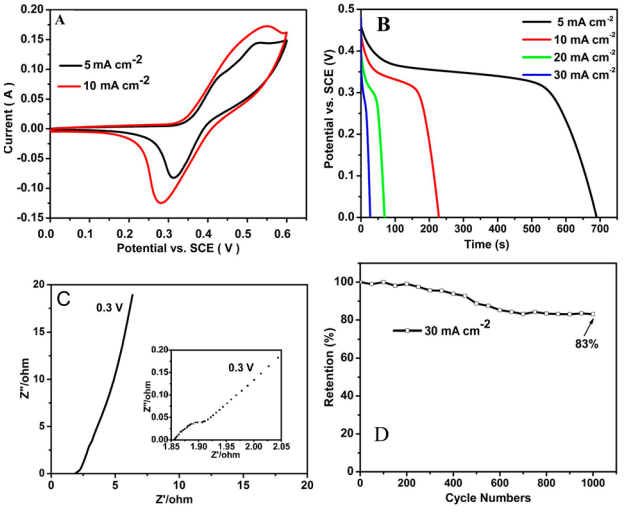

Figure 6. Electrochemical measurements of the NiAl−LDH/MWCNT/NF electrode. (A) CV curves recorded at scan rates of 5 and 10 mV s^{-1}. (B) Galvanostatic discharge curves. (C) Nyquist plots, measured at 0.3 V, with an inset illustrating the high frequency region. (D) Specific capacitance retention as a function of cycle number (galvanostatic charge/discharge current densities are 30 mA cm^{-2}).

The specific capacitance is calculated as

$$C = \frac{I \times \Delta t}{\Delta V \times m} \quad (2)$$

and areal capacitance as

$$C_a = \frac{I \times \Delta t}{\Delta V \times S} \quad (3)$$

where I, Δt, ΔV, m, and S are the discharge current, discharge time, voltage drop upon discharging (excluding the sudden potential drop), the mass of the active material (LDH), and the geometrical area of the electrode, respectively. The areal capacitance (C_a) of the NiAl−LDH/MWCNT/NF electrode was calculated to be 7.5, 5.2, 3.4, and 2.3 F cm^{-2} at charge and discharge current densities of 5, 10, 20, and 30 mA cm^{-2}, respectively (Figure 6B). The mass specific capacitance (C) was determined to be approximately 1293 F g^{-1} (based on the mass of NiAl−LDH) at 5 mA cm^{-2}. The Nyquist plot of the NiAl−LDH/MWCNT/NF electrode measured at 0.3 V in the frequency range of 0.01−10^5 Hz is presented in Figure 6C. The Nyquist plot is composed of three regions. In the high frequency region, a depressed semicircle may be seen. This arises because of two concomitantly occurring processes: charge-transfer resistance and the double-layer capacitance. The internal resistance of the electrode under open circuit conditions is found to be approximately 1.85 Ω (R_s). The crossover point where the highest frequency meets the real part of the impedance reflects the amalgamation of the electrolyte resistance, the substrate's intrinsic resistance of substrate, and contact resistance that exists between the active material and the current collector. In the high frequency region, a semicircle reflecting the charge-transfer resistance (R_{ct}) can be seen (∼0.13 Ω), which is attributed to the charge-transfer resistance at the electrode/electrolyte interface.[48−51] At the intermediate frequency range, a straight line with a gradient close to 45° is observed. This is symptomatic of ion diffusion into the electrode. In the low frequency range, the straight line is tilted toward the imaginary axis: this shows that the electrolyte has good capacitance. This can be explained because the large pores in the material lead to high ionic mobility.[49] The NiAl−LDH/MWCNT/NF electrode demonstrates not only a high specific capacitance and low resistance but also remarkable cycling stability. The results of repeated charge−discharge cycling at 30 mA cm^{-2} are given in Figure 6D. After 1000 cycles, the capacitance remained at 83% of its initial value. This clearly indicates that the NiAl−LDH/MWCNT/NF electrode can provide highly reliable capacitive performance at elevated charge/discharge rates for power-hungry applications.

The electrochemical characterization data for the NiAl−LDH film deposited directly on Ni foam are included in Figure 7. The C_a was 5.6 F cm^{-2} and C was 938 F g^{-1} at 5 mA cm^{-2} (Figure 7A). These values are much lower than those for the NiAl−LDH/MWCNT/NF electrode. Cycling charge−discharge testing indicated that, after 1000 cycles, the capacitance was reduced to at 69% of its initial value (Figure 7D), again a lower value than that with the NiAl−LDH/MWCNT/NF electrode. The Nyquist plot of the NiAl−LDH film demonstrates a similar shape to that of the NiAl−LDH/MWCNT/NF sample, with a semicircle at the higher frequency region and a spike at lower frequency. The R_s and R_{ct} of the NiAl−LDH film electrode were calculated to be ca. 1.90 and 0.84 Ω, respectively (Figure 7C). The NiAl−LDH/MWCNT/NF material has a much smaller R_{ct} (∼0.13 Ω) in addition to a similarly small R_s, indicative of its enhanced electrical conductivity and electroactivity. An MWCNT/NF film was also tested as electrode materials using CVs and EIS (Figure 8). Obviously, the C of MWCNT/NF film (Figure 8A) is far less than that of NiAl−LDH/MWCNT/NF film (Figure 6A).

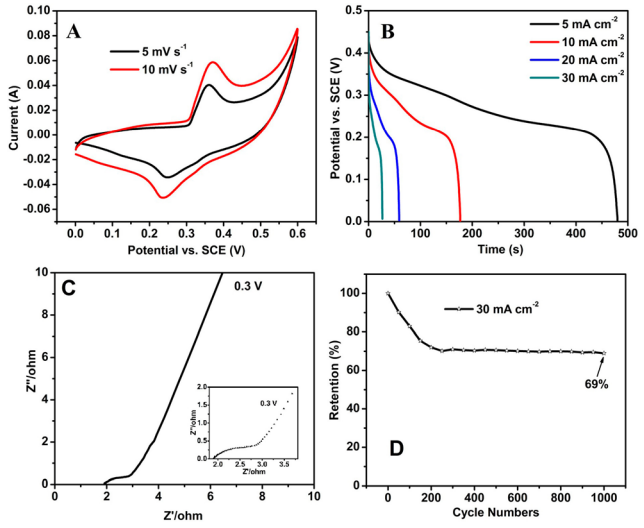

Figure 7. Electrochemical measurements of the NiAl–LDH film grown directly on a Ni foam. (A) CV curves at scan rates of 5 and 10 mV s^{-1}. (B) Galvanostatic discharge curves). (C) Nyquist plots obtained at 0.3 V, with an inset depicting the high frequency region. (D) Specific capacitance retention as a function of cycle number (data were obtained at galvanostatic charge/discharge current densities of 30 mA cm^{-2}).

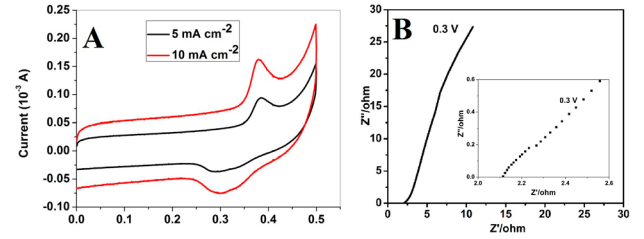

Figure 8. Electrochemical measurements of the MWCNT/NF. (A) CV curves at different scan rates (5 and 10 mV s^{-1}), and (B) Nyquist plots measured at 0.3 V. The inset is the high frequency region.

Therefore, the MWCNT has a very little attribution to the capacity of NiAl–LDH/MWCNT/NF film. However, the R_{ct} of the MWCNT/NF film is about 0.21 Ω (Figure 8B), indicating that MWCNT has great contributions to the electrical conductivity and electroactivity of NiAl–LDH/MWCNT/NF film. This demonstrates that more facile charge transfer is achieved by integrating NiAl–LDH platelets onto the tubular MWCNT. The higher specific capacitance of the NiAl–LDH/MWCNT/NF electrode may be attributed to more effective exploitation of the NiAl–LDH platelets on the highly conductive MWCNT. The 3D hierarchical NiAl–LDH/MWCNT/NF structure enhanced the active surface area and improved the transport of ions, facilitating surface-dependent Faradaic processes.[52,53] The specific capacitance observed, 1293 F g^{-1} (7.5 F cm^{-2}) at a current density of 5 mA cm^{-2}, is among the highest that has been reported for oxide/hydroxide derived architectures. Such values have previously been seen with NiTi–LDH/NF film (10.37 F cm^{-2}),[33] β-$Ni(OH)_2$/NF (2675 F g^{-1}),[34] hierarchical $Ni_{0.25}Co_{0.75}(OH)_2$ (928.4 F g^{-1} or 9.59 F cm^{-2}),[35] hybrid nickel hydroxide/carbon nanotubes (16 F cm^{-2}),[39] and 3D nanostructures of CoO@$Ni(OH)_2$ (11.49 F cm^{-2}).[8] As a result of its excellent capacitive performance and ease of fabrication, the NiAl–LDH/MWCNT/NF film developed in this work comprises a promising alternative to nickel-based oxide/hydroxide materials for next-generation supercapacitors.

4. CONCLUSIONS

In summary, a well-defined 3D hierarchical NiAl layered double hydroxide/multiwalled carbon nanotube/Ni foam (NiAl–LDH/MWCNT/NF) electrode with high capacitance has been efficiently synthesized by a facile three-step method. The NiAl–LDH was uniformly dispersed on the MWCNT surface. A high specific capacitance of 1293 F g^{-1} was achieved at a current density of 5 mA cm^{-2}. The electrode showed good cycling performance, with 83% of the initial specific capacitance retained after 1000 cycles. The NiAl–LDH/MWCNT/NF electrode had a much higher specific capacitance and better cycling stability than a NiAl–LDH film grown directly on Ni foam. This method of hierarchical architecture preparation can easily be extended to other transition-metal-based oxide/hydroxide systems to enhance their capacitance.

AUTHOR INFORMATION

Corresponding Author

*Tel: +861064455357. Fax: +861064425385. E-mail: leixd@mail.buct.edu.cn (X.L.).

Notes

The authors declare no competing financial interest.

ACKNOWLEDGMENTS

This research project was financially supported by the 973 Program (No. 2014CB932104), the 863 Program (No. 2012AA03A609), NSFC, and the Program for Changjiang Scholars and Innovative Research Team in University (No. IRT1205) of People's Republic of China.

REFERENCES

(1) Simon, P.; Gogotsi, Y. Materials for Electrochemical Capacitors. *Nat. Mater.* **2008**, *7*, 845–854.
(2) Miller, J. R.; Simon, P. Electrochemical Capacitors for Energy Management. *Science* **2008**, *321*, 651–652.
(3) Zhang, H.; Yu, X.; P. Braun, V. Three-Dimensional Bicontinuous Ultrafast-Charge and -Discharge Bulk Battery Electrodes. *Nat. Nanotechnol.* **2011**, *6*, 277–281.
(4) Zhu, Y.; Murali, S.; Stoller, M. D.; Ganesh, K.; Cai, W.; Ferreira, P. J.; Pirkle, A.; Wallace, R. M.; Cychosz, K. A.; Thommes, M.; Su, D.; Stach, E. A.; Ruoff, R. S. Carbon-Based Supercapacitors Produced by Activation of Graphene. *Science* **2011**, *332*, 1537–1541.
(5) Liu, C.; Li, F.; Ma, L. P.; Cheng, H. M. Advanced Materials for Energy Storage. *Adv. Mater.* **2010**, *22*, E28–E62.
(6) Ho, G. W.; Wong, A. S. W. One Step Solution Synthesis Towards Ultra-Thin and Uniform Single-Crystalline ZnO Nanowires. *Appl. Phys. A: Mater. Sci. Process.* **2007**, *86*, 457–462.
(7) Jiang, J.; Li, Y.; Liu, J.; Huang, X. Building One-Dimensional Oxide Nanostructure Arrays on Conductive Metal Substrates for Lithium-Ion Battery Anodes. *Nanoscale* **2011**, *3*, 45–58.
(8) Guan, C.; Li, X.; Wang, Z.; Cao, X.; Soci, C.; Zhang, H.; Fan, H. J. Nanoporous Walls on Macroporous Foam: Rational Design of Electrodes to Push Areal Pseudocapacitance. *Adv. Mater.* **2012**, *24*, 4186–4190.
(9) Cao, C.-Y.; Guo, W.; Cui, Z.-M.; Song, W.-G.; Cai, W. Microwave-Assisted Gas/Liquid Interfacial Synthesis of Flowerlike NiO Hollow Nanosphere Precursors and Their Application as Supercapacitor Electrodes. *J. Mater. Chem.* **2011**, *21*, 3204–3209.
(10) Dong, X.-C.; Xu, H.; Wang, X.-W.; Huang, Y.-X.; Chan-Park, M. B.; Zhang, H.; Wang, L.-H.; Huang, W.; Chen, P. 3D Graphene-Cobalt Oxide Electrode for High-Performance Supercapacitor and Enzyme-less Glucose Detection. *ACS Nano* **2012**, *6*, 3206–3213.

(11) Xia, X.-H.; Tu, J.-P.; Wang, X.-L.; Gu, C.-D.; Zhao, X.-B. Mesoporous Co_3O_4 Monolayer Hollow-Sphere Array as Electrochemical Pseudocapacitor Material. *Chem. Commun.* **2011**, *47*, 5786−5788.
(12) Wang, G.; Liu, H.; Horvat, J.; Wang, B.; Qiao, S.; Park, J.; Ahn, H. Highly Ordered Mesoporous Cobalt Oxide Nanostructures: Synthesis, Characterisation, Magnetic Properties, and Applications for Electrochemical Energy Devices. *Chem.—Eur. J.* **2010**, *16*, 11020−11027.
(13) Tang, X.; Liu, Z.-H.; Zhang, C.; Yang, Z.; Wang, Z. Synthesis and Capacitive Property of Hierarchical Hollow Manganese Oxide Nanospheres with Large Specific Surface Area. *J. Power Sources* **2009**, *193*, 939−943.
(14) Zang, J.; Bao, S.-J.; Li, C. M.; Bian, H.; Cui, X.; Bao, Q.; Sun, C. Q.; Guo, J.; Lian, K. Well-Aligned Cone-Shaped Nanostructure of Polypyrrole/RuO_2 and Its Electrochemical Supercapacitor. *J. Phys. Chem. C* **2008**, *112*, 14843−14847.
(15) Hu, Z.-A.; Xie, Y.-L.; Wang, Y.-X.; Xie, L.-J.; Fu, G.-R.; Jin, X.-Q.; Zhang, Z.-Y.; Yang, Y.-Y.; Wu, H.-Y. Synthesis of α-Cobalt Hydroxides with Different Intercalated Anions and Effects of Intercalated Anions on Their Morphology, Basal Plane Spacing, and Capacitive Property. *J. Phys. Chem. C* **2009**, *113*, 12502−12508.
(16) Yang, G.-W.; Xu, C.-L.; Li, H.-L. Electrodeposited Nickel Hydroxide on Nickel Foam with Ultrahigh Capacitance. *Chem. Commun.* **2008**, 6537−6539.
(17) Yang, S.; Wu, X.; Chen, C.; Dong, H.; Hu, W.; Wang, X. Spherical α-$Ni(OH)_2$ Nanoarchitecture Grown on Graphene as Advanced Electrochemical Pseudocapacitor Materials. *Chem. Commun.* **2012**, *48*, 2773−2775.
(18) Wang, H.; Casalongue, H. S.; Liang, Y. Y.; Dai, H. $Ni(OH)_2$ Nanoplates Grown on Graphene as Advanced Electrochemical Pseudocapacitor Materials. *J. Am. Chem. Soc.* **2010**, *132*, 7472−7477.
(19) Wang, Y.-G.; Wang, Z.-D.; Xia, Y.-Y. An Asymmetric Supercapacitor Using RuO_2/TiO_2 Nanotube Composite and Activated Carbon Electrodes. *Electrochim. Acta* **2005**, *50*, 5641−5646.
(20) Kong, L.-B.; Lang, J.-W.; Liu, M.; Luo, Y.-C.; Kang, L. Facile Approach to Prepare Loose-Packed Cobalt Hydroxide Nano-Flakes Materials for Electrochemical Capacitors. *J. Power Sources* **2009**, *194*, 1194−1201.
(21) Pang, S.-C.; Anderson, M. A.; Chapman, T. W. Novel Electrode Materials for Thin-Film Ultracapacitors: Comparison of Electrochemical Properties of Sol-Gel-Derived and Electrodeposited Manganese Dioxide. *J. Electrochem. Soc.* **2000**, *147*, 444−450.
(22) Nam, K.-W.; Kim, K.-B. A Study of the Preparation of NiO_x Electrode via Electrochemical Route for Supercapacitor Applications and Their Charge Storage Mechanism. *J. Electrochem. Soc.* **2002**, *149*, A346−A354.
(23) Tang, C.-H.; Yin, X.; Gong, H. Superior Performance Asymmetric Supercapacitors Based on a Directly Grown Commercial Mass 3D Co_3O_4@$Ni(OH)_2$ Core−Shell Electrode. *ACS Appl. Mater. Interfaces* **2013**, *5*, 10574−10582.
(24) Liu, J.; Jiang, J.; Cheng, C.; Li, H.; Zhang, J.; Gong, H.; Fan, H. J. Co_3O_4 Nanowire@MnO_2 Ultrathin Nanosheet Core/Shell Arrays: A New Class of High-Performance Pseudocapacitive Materials. *Adv. Mater.* **2011**, *23*, 2076−2081.
(25) Xia, X.; Tu, J.; Zhang, Y.; Wang, X.; Gu, C.; Zhao, X.-B.; Fan, H. J. High-Quality Metal Axide Core/Shell Nanowire Arrays on Conductive Substrates for Electrochemical Energy Storage. *ACS Nano* **2012**, *6*, 5531−5538.
(26) Zhang, T.; Li, Q.; Xiao, H.; Lu, H.; Zhou, Y. Synthesis of Li-Al Layered Double Hydroxides (LDHs) for Efficient Fluoride Removal. *Ind. Eng. Chem. Res.* **2012**, *51*, 11490−11498.
(27) Velu, S.; Suzuki, K.; Kapoor, M. P.; Tomura, S.; Ohashi, F.; Osaki, T. Effect of Sn Incorporation on the Thermal Transformation and Reducibility of M(II)Al-Layered Double Hydroxides [M(II) = Ni or Co]. *Chem. Mater.* **2000**, *12*, 719−730.
(28) Shu, X.; He, J.; Chen, D.; Wang, Y. Tailoring of Phase Composition and Photoresponsive Properties of Ti-Containing Nanocomposites from Layered Precursor. *J. Phys.Chem. C* **2008**, *112*, 4151−4158.
(29) Lu, Z.; Zhu, W.; Lei, X.; Williams, G. R.; O'Hare, D.; Chang, Z.; Sun, X.; Duan, X. High Pseudocapacitive Cobalt Carbonate Hydroxide Films Derived from CoAl Layered Double Hydroxides. *Nanoscale* **2012**, *4*, 3640−3643.
(30) Wang, Y.; Yang, W.; Chen, C.; Evans, D. G. Fabrication and Electrochemical Characterization of Cobalt-Based Layered Double Hydroxide Nanosheet Thin-Film Electrodes. *J. Power Sources* **2008**, *184*, 682−690.
(31) Wang, B.; Liu, Q.; Qian, Z.; Zhang, X.; Wang, J.; Li, Z.; Yan, H.; Gao, Z.; Zhao, F.; Liu, L. Two Steps *in Situ* Structure Fabrication of Ni−Al Layered Double Hydroxide on Ni Foam and Its Electrochemical Performance for Supercapacitors. *J. Power Sources* **2014**, *246*, 747−753.
(32) Gao, Z.; Wang, J.; Li, Z.; Yang, W.; Wang, B.; Hou, M.; He, Y.; Liu, Q.; Mann, T.; Yang, P.; Zhang, M.; Liu, L. Graphene Nanosheet/Ni^{2+}/Al^{3+} Layered Double-Hydroxide Composite as a Novel Electrode for a Supercapacitor. *Chem. Mater.* **2011**, *23*, 3509−3516.
(33) Gu, Y.; Lu, Z.; Chang, Z.; Liu, J.; Lei, X.; Li, Y.; Sun, X. NiTi Layered Double Hydroxide Thin Films for Advanced Pseudocapacitor Electrodes. *J. Mater. Chem. A* **2013**, *1*, 10655−10661.
(34) Lu, Z.; Chang, Z.; Zhu, W.; Sun, X. Beta-Phased $Ni(OH)_2$ Nanowall Film With Reversible Capacitance Gigher Than Theoretical Faradic Capacitance. *Chem. Commun.* **2011**, *47*, 9651−9653.
(35) Zhu, W.; Lu, Z.; Zhang, G.; Lei, X.; Chang, Z.; Liu, J.; Sun, X. Hierarchical $Ni_{0.25}Co_{0.75}(OH)_2$ Nanoarrays for a High-Performance Supercapacitor Electrode Prepared by an *in Situ* Conversion Process. *J. Mater. Chem. A* **2013**, *1*, 8327−8331.
(36) Yang, Q.; Lu, Z.; Chang, Z.; Zhu, W.; Sun, J.; Liu, J.; Sun, X.; Duan, X. Hierarchical Co_3O_4 Nanosheet@Nanowire Arrays with Enhanced Pseudocapacitive Performance. *RSC Adv.* **2012**, *2*, 1663−1668.
(37) Liu, X.; Wang, C.; Dou, Y.; Zhou, A.; Pan, T.; Han, J.; Wei, M. A NiAl Layered Double Hydroxide@Carbon Nanoparticles Hybrid Electrode for High-Performance Asymmetric Supercapacitors. *J. Mater. Chem. A* **2014**, *2*, 1682−1685.
(38) Zhao, M.; Zhang, Q.; Huang, J.; Wei, F. Hierarchical Nanocomposites Derived from Nanocarbons and Layered Double Hydroxides - Properties, Synthesis, and Applications. *Adv. Funct. Mater.* **2012**, *22*, 675−694.
(39) Tang, Z.; Tang, C.-H.; Gong, H. A High Energy Density Asymmetric Supercapacitor from Nano-architectured $Ni(OH)_2$/Carbon Nanotube Electrodes. *Adv. Funct. Mater.* **2012**, *22*, 1272−1278.
(40) Zhang, L.; Li, F.; Xiang, X.; Wei, M.; Evans, D. G. Ni-Based Supported Catalysts from Layered Double Hydroxides: Tunable Microstructure and Controlled Property for the Synthesis of Carbon Nanotubes. *Chem. Eng. J.* **2009**, *155*, 474−482.
(41) Dresselhaus, M. S.; Dresselhaus, G.; Saito, R.; Jorio, A. Raman Spectroscopy of Carbon Nanotubes. *Phys. Rep.* **2005**, *409*, 47−99.
(42) Dresselhaus, M. S.; Dresselhaus, G.; Jorio, A. Unusual Properties and Structure of Carbon Nanotubes. *Annu. Rev. Mater. Res.* **2004**, *34*, 247−278.
(43) Zhao, Y.; He, S.; Wei, M.; Evans, D. G.; Duan, X. Hierarchical Films of Layered Double Hydroxides by Using a Sol-Gel Process and Their High Adaptability in Water Treatment. *Chem. Commun.* **2010**, *46*, 3031−3033.
(44) Wang, J.; Song, Y.; Li, Z.; Liu, Q.; Zhou, J.; Jing, X.; Zhang, M.; Jiang, Z. *In Situ* Ni/Al Layered Double Hydroxide and Its Electrochemical Capacitance Performance. *Energy Fuels* **2010**, *24*, 6463−6467.
(45) Prevot, V.; Forano, C.; Besse, J. P. Hydrolysis in Polyol: New Route for Hybrid-Layered Double Hydroxides Preparation. *Chem. Mater.* **2005**, *17*, 6695−6701.
(46) Caravaggio, G. A.; Detellier, C.; Wronski, Z. Synthesis, Stability and Electrochemical Properties of NiAl And NiV Layered Double Hydroxides. *J. Mater. Chem.* **2001**, *11*, 912−921.

(47) Nam, K.-W.; Kim, K.-H.; Lee, E.-S.; Yoon, W.-S.; Yang, X.-Q.; Kim, K.-B. Pseudocapacitive Properties of Electrochemically Prepared Nickel Oxides on 3-Dimensional Carbon Nanotube Film Substrates. *J. Power Sources* **2008**, *182*, 642−652.
(48) Cui, L.; Li, J.; Zhang, X. Preparation and Properties of Co_3O_4 Nanorods as Supercapacitor Material. *J. Appl. Electrochem.* **2009**, *39*, 1871−1876.
(49) Xu, J.; Gao, L.; Cao, J.; Wang, W.; Chen, Z. Preparation and Electrochemical Capacitance of Cobalt Oxide (Co_3O_4) Nanotubes as Supercapacitor Material. *Electrochim. Acta* **2010**, *56*, 732−736.
(50) Yuan, A.; Zhang, Q. A Novel Hybrid Manganese Dioxide/Activated Carbon Supercapacitor Using Lithium Hydroxide Electrolyte. *Electrochem. Commun.* **2006**, *8*, 1173−1178.
(51) Liu, J.; Jiang, J.; Bosmanc, M.; Fan, H. J. Three-Dimensional Tubular Arrays of MnO_2−NiO Nanoflakes with High Areal Pseudocapacitance. *J. Mater. Chem.* **2012**, *22*, 2419−2426.
(52) Kamath, P. V.; Therese, G. H. A.; Gopalakrishnan, J. On the Existence of Hydrotalcite-Like Phases in the Absence of Trivalent Cations. *J. Solid State Chem.* **1997**, *128*, 38−41.
(53) Portemer, F.; Delahaye-Vidal, A.; Figlarz, M. Characterization of Active Material Deposited at the Nickel Hydroxide Electrode by Electrochemical Impregnation. *J. Electrochem. Soc.* **1992**, *139*, 671−678.